Chapter 18

ELECTRON-PROTON INSTABILITY

18.1 INTRODUCTION

An intense particle beam forms a potential well for oppositely charged particles and will therefore trap particles of opposite sign. These trapped particles can often accumulate to each an extent that they provide a potential well for particles of the original beam. Thus, the secondary beam can oscillate transversely in the potential well of the primary beam and the primary beam can oscillate transversely in the potential well of the secondary beam. This coupled beam oscillation may grow in amplitude and lead to beam loss eventually. This is called two-stream instability.

Proton beam trapping electrons has first been observed in the Bevatron [1] and later in the CERN ISR [2]. The ISR is a collider with an intense coasting proton beam in each of the intersecting vacuum chambers. It has been observed that electrons were trapped in the potential of the proton beams with oscillation frequency around 100 MHz. The instability is intermittent. It stops when the electrons, driven to large amplitudes, are shaken out to the walls, or out of resonance with the protons. It restarts when a sufficient number of new electrons has been accumulated. Slow beam blow-up and background problems are the result.

The PSR at Los Alamos (LANL) running with 2.3 to 4.2×10^{13} protons has always

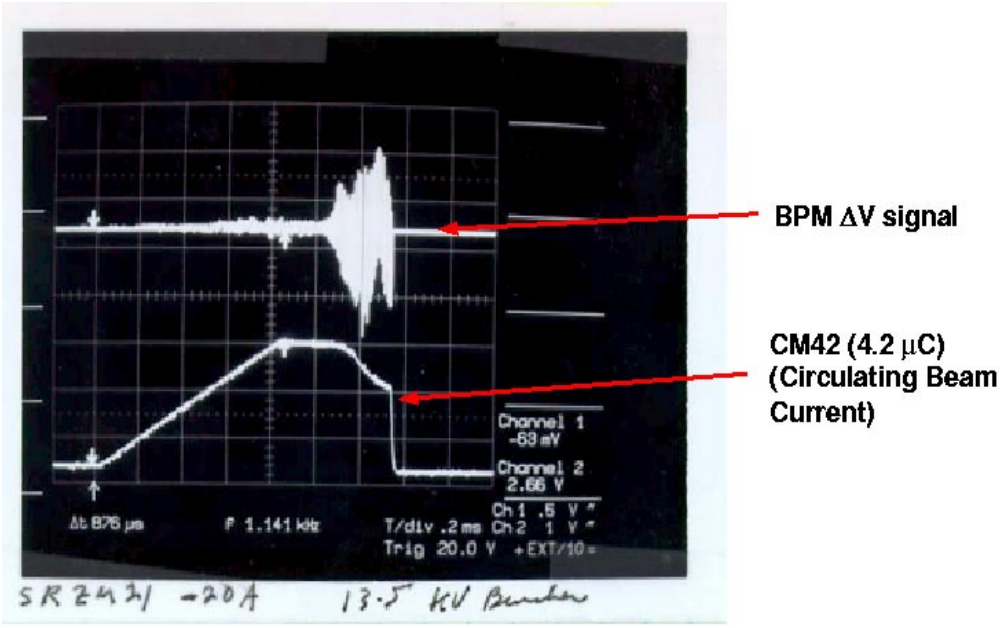

Figure 18.1: Top trace: vertical difference signal of the beam reveals a growing instability about 300 μs after the end of injection. Lower trace: sum signal of the beam showing beam loss as the instability grows.

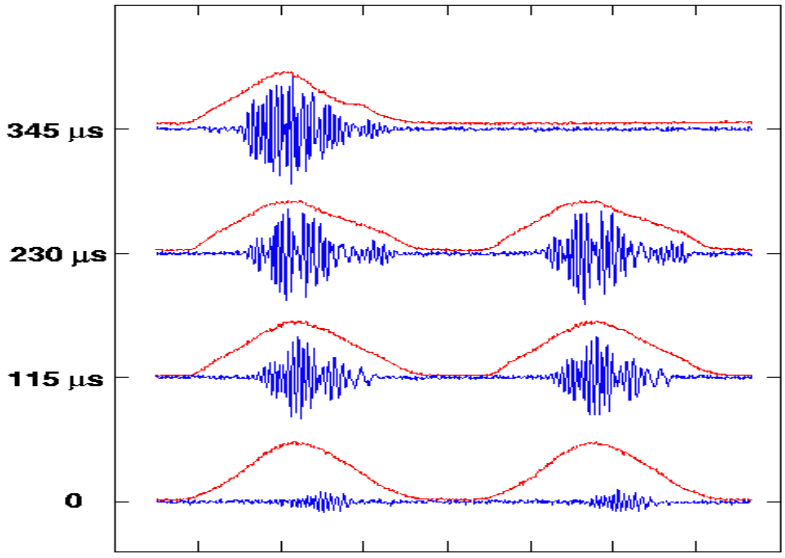

Figure 18.2: Turn-by-turn vertical difference signals from a short stripline BPM at the final 300 μs of the store show a vertical instability starting at the back end of the bunch and spreading into the whole bunch with increasing amplitude. The bunch sum profiles from a wall current monitor are also shown revealing a beam loss as the instability develops.

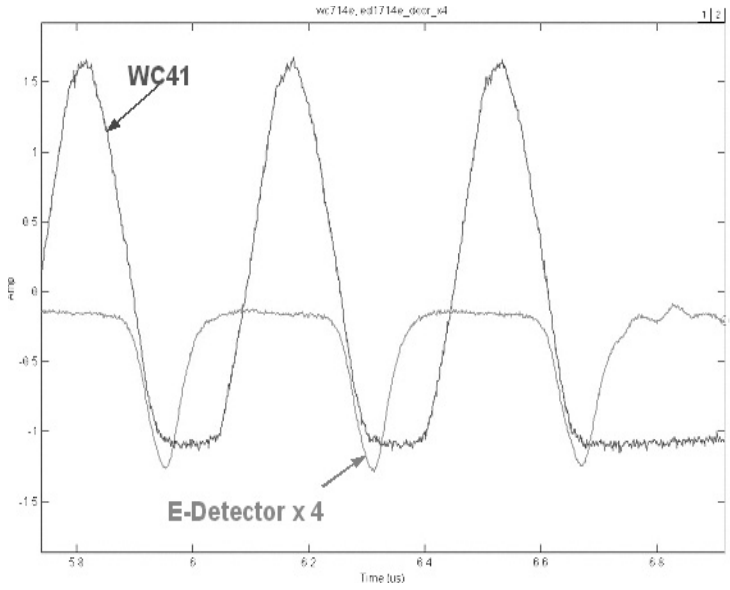

Figure 18.3: Turn-by-turn electron signal is shown in relation to the proton beam pulse at PSR. Electrons start to appear at the back end of the beam pulse.

been troubled by the electrons trapped inside the proton beam [3]. A turn by turn picture of the electron signal in relation to the circulating beam pulse at the end of a 500 ms store of stable beam is shown in Fig. 18.3. The timing between electrons and proton beam is good to a few ns. The electron detector was designed and built at ANL. It has a repeller grid, so that it can decouple the electron energy analysis from collection. The repeller voltage of 5 volts means the electrons have to be above 5 eV in order to get through to the collector. Electrons start to appear after the peak of the beam pulse has passed and the peak of the electrons appears at the end of the beam pulse. Higher repeller voltage shows a smaller, and narrower pulse.

An instability is clearly seen when beam is stored for about 300 microseconds after the end of injection. A rapidly growing vertical difference signal (top trace) can be seen shortly before the beam loss lower trace, indicating the beam centroid oscillation. In Fig. 18.2, the growth of the instability can be seen turn by turn at the final $\sim$ 300 μs of the store. Here the vertical difference signal is compared to the wall current monitor trace. The beam transverse instability starts on the backside of the pulse and broadens out as it grows in strength. Some beam loss is evident at the last turn before extraction.

The Brookhaven booster running in the coasting beam mode suffers sudden beam loss due to a vertical instability [4], which cannot be identified with any reasonable amount

of transverse impedance. This has been considered to be the result of e-p instability.

The Fermilab antiproton ring traps positive ions and limits the intensity of the storage [5]. The newly built APS at ANL is a synchrotron light source using a positron beam. It has been observed that electrons are trapped causing instability [6].

18.2 SINGLE-ELECTRON MECHANICS

Coupled-centroid oscillation of the proton beam and the trapped electron beam will occur only when the amount of electrons becomes very intense. Therefore, to prevent such instability, we would like the electrons in the vacuum chamber not to accumulate. The electrons inside the vacuum chamber are supposed not to move longitudinally. As the proton bunch passes through them, they are attracted towards the central axis of the proton bunch with vertical electron *bounce frequency* $\Omega_e/(2\pi)$ given by [11]

$$\Omega_e^2 = \frac{4Nr_ec^2}{a_V(a_V + a_H)L_b} \ . \tag{18.1}$$

Here, N_p is the number of protons in the bunch which has an elliptical cross section with vertical and horizontal radii a_V and a_H, L_b is the full bunch length, and r_e the electron classical radius. We assume that the proton beam has uniform longitudinal and radial distribution and has a cylindrical cross section with radius a inside a cylindrical beam pipe of radius b. Thus $a_V(a_V + a_H)$ can be replaced by $2a^2$. The images of the proton beam and the electron cloud in the walls of the vacuum chamber will modify the electron bounce frequency depicted in Eq. (18.1), but their effects are neglected in this study. Also, only linear focusing force by the proton beam on the electrons is considered.

An electron trapped inside the proton beam performs betatron oscillations with an equivalent betatron function $\beta_b = \beta c/\Omega_e$ with a total betatron phase advance $\phi_b = \Omega_e L_b/v$, where βc is the velocity of the protons. After the passage of the proton bunch, the motion of the electron in the gap is equivalent to a drift of length $L_g = \lambda_{\rm rf} - L_b$ with $\lambda_{\rm rf}$ being the rf wavelength or stationary bucket width. Here, we assume all rf buckets are filled. The transfer matrix for an rf wavelength is [7]

$$M = \begin{pmatrix} 1 & L_g \\ 0 & 1 \end{pmatrix} \begin{pmatrix} \cos\phi_b & \beta_b \sin\phi_b \\ -\dfrac{1}{\beta_b}\sin\phi_b & \cos\phi_b \end{pmatrix} = \begin{pmatrix} \cos\phi_b - \dfrac{L_g}{\beta_b}\sin\phi_b & \beta_b\sin\phi_b + L_g\sin\phi_b \\ -\dfrac{1}{\beta_b}\sin\phi_b & \cos\phi_b \end{pmatrix} . \tag{18.2}$$

Table 18.1: Some data of the Oak Ridge SNS, the Los Alamos PSR, and the Brookhaven booster at injection.

	Oak Ridge SNS	Los Alamos PSR	Brookhaven Booster
Circumference C (m)	220.6880	90.2000	201.769
Injection kinetic energy (GeV)	1.000	0.797	0.200
γ	2.0658	1.8494	1.2132
β	0.8750	0.8412	0.5662
Revolution frequency f_0 (MHz)	1.1887	2.7959	0.8412
Revolution period T_0 (ns)	841.3	357.7	1189
Total number of protons N_p	2.1×10^{14}	4.2×10^{13}	2.4×10^{13}
Rf harmonic (no. of bunches) h	1	1	1
Number of injection turns	1225	2000	300
Repetition rate (Hz)	60	12	7.5

In order that the electron will not be trapped inside the proton bunch, its motion has to be unstable or

$$\frac{1}{2}|\mathrm{Tr}M| = \left|\cos\phi_b - \frac{L_g}{2\beta_b}\sin\phi_b\right| > 1 \ . \tag{18.3}$$

If the electron is unstable, we can write

$$\frac{1}{2}|\mathrm{Tr}M| = \cosh\mu \ , \tag{18.4}$$

where $\mu\beta c/\lambda_{\rm rf}$ is the growth rate of the electron oscillation amplitude, and μ^{-1} is the growth time in rf buckets. Here, we study the effect of trapped electrons in the 3 rings: the SNS spallation storage ring to be built at Oak Ridge (ORNL), the Los Alamos PSR, and the booster at Brookhaven (BNL). Some information of the three rings are listed in Table 18.1.

Equation (18.3) appears to be a simple criterion. In fact, it is much more complex, because the electron bounce frequency turns out to be usually a large number. Take for example the PSR, we find $\Omega_e = 1.254$ GHz, which gives an equivalent betatron function $\beta_b = \beta c/\Omega_e = 0.201$ m. With the gap length 30.07 m, $L_g/\beta_b = 150$. Although Ω_e is not sensitive to L_g/β_b, it is very sensitive to the phase $\phi_b = \Omega_e L_g/v \approx 299$ rad and therefore to $\sin\phi_b$ and $\cos\phi_b$. Thus, a very slight change in the number of protons in the beam will alter the electron bounce frequency, the betatron phase, and give rise to a large change

Table 18.2: Instability and escape time through the bunch gap of a single electron trapped inside the proton bunches of the ORNL SNS, LANL PSR, and BNL booster.

	Oak Ridge SNS	Los Alamos PSR	Brookhaven Booster
Injection full bunch length (m)	143.39	60.13	100.89
Gap length (m)	77.30	30.07	100.89
Proton beam radius a (m)	0.0380	0.0150	0.0150
Bounce angular frequency Ω_e (MHz)	713.3	1253.9	462.6
Bounce betatron phase ϕ_b (rad)	309.9	299.0	435.2
$\frac{1}{2}\|\mathrm{Tr}M\|$ (rms)	52.55	37.38	108.8
Escape time in no. of rf buckets	0.2148	0.2318	0.1858

in the trace. Since the electron bounce frequency usually has a large spread, it is more reasonable to consider the rms value of the trace instead.

The results of $\frac{1}{2}|\mathrm{Tr}M|$ are listed in Table 18.2. We see that for all the 3 rings, the electrons trapped should be able to escape to the walls of the beam pipe in the beam gap. In fact, with such high electron bounce frequency, L_g/β_b will be large, it will not be easy to trap any electrons if the gap is clean. When the intensity of the proton beam is raised, the electron bounce frequency will increase, making the electrons easier to escape at the gap.

Sometimes, the gap is not totally free of protons. The space-charge effect of the protons will distort the rf bucket reducing its momentum acceptance. As a result, some protons may leak out of the bucket and end up in the bunch gap. If a fraction η of the protons leaks into the gap, the electron will oscillate with bounce frequency $\Omega_{eb}/(2\pi)$ inside the proton beam and bounce frequency $\Omega_{eg}/(2\pi)$ in the bunch gap. These frequencies are given by [7, 9]

$$\Omega_{eb}^2 = \Omega_e^2(1-\eta) \qquad \text{and} \qquad \Omega_{eg}^2 = \Omega_e^2\eta\frac{L_b}{L_g}\ . \tag{18.5}$$

Again, only linear focusing force by the proton beam is considered. The betatron phase advances in the beam and in the gap are, respectively, $\phi_b = \Omega_{eb}L_b/(\beta c)$ and $\phi_g = \Omega_{eb}L_g/(\beta c)$. The transfer matrix is therefore

$$M = \begin{pmatrix} \cos\phi_g & \beta_g\sin\phi_g \\ -\dfrac{1}{\beta_g}\sin\phi_g & \cos\phi_g \end{pmatrix}\begin{pmatrix} \cos\phi_b & \beta_b\sin\phi_b \\ -\dfrac{1}{\beta_b}\sin\phi_b & \cos\phi_b \end{pmatrix}$$

$$= \begin{pmatrix} \cos\phi_g\cos\phi_b - \dfrac{\beta_g}{\beta_b}\sin\phi_g\sin\phi_b & \beta_b\cos\phi_g\sin\phi_b + \beta_g\cos\phi_b\sin\phi_g \\ -\dfrac{1}{\beta_g}\cos\phi_b\sin\phi_g - \dfrac{1}{\beta_b}\cos\phi_g\sin\phi_b & -\dfrac{\beta_b}{\beta_g}\sin\phi_b\sin\phi_g + \cos\phi_g\cos\phi_b \end{pmatrix} , \quad (18.6)$$

where the equivalent betatron functions in the bunch and in the gap are, respectively,

$$\beta_b = \frac{\beta c}{\Omega_{eb}} \qquad \text{and} \qquad \beta_g = \frac{\beta c}{\Omega_{eg}} . \quad (18.7)$$

The condition for the electrons to escape is therefore

$$\frac{1}{2}|\mathrm{Tr}M| = \left|\cos\phi_g\cos\phi_b - \frac{1}{2}\left(\frac{\Omega_{eb}}{\Omega_{eg}} + \frac{\Omega_{eg}}{\Omega_{eb}}\right)\sin\phi_g\sin\phi_b\right| > 1 . \quad (18.8)$$

It is easy to demonstrate that Eq. (18.8) becomes Eq. (18.3) when $\eta \to 0$.

Figure 18.4 show $\frac{1}{2}\mathrm{Tr}M$ as a function of the fractional proton leakage η into the gap, respectively, for the ORNL SNS, LANL PSR, and BNL Booster. The plots for the ORNL SNS and LANL PSR are very similar; $\frac{1}{2}\mathrm{Tr}M$ oscillates rapidly with the fractional leakage and becomes bounded by ± 1 or electrons will be trapped when $\eta \gtrsim 0.05$. The situation for the BNL booster is different. Even up to $\eta = 0.20$, the oscillation of $\frac{1}{2}\mathrm{Tr}M$ still has an amplitude larger than 1. This is mainly due to the fact of a larger gap-to-bunch-length ratio in the BNL Booster. Thus, we may conclude that electrons are not so easily trapped in BNL booster as in the ORNL SNS and LANL PSR when protons are spilled into the bunch gaps. We also try to vary the electron bounce frequency in each case and find that the results remain relatively the same. The only changes in the plots are faster oscillations when the bounce frequency is increased.

18.3 CENTROID-OSCILLATION INSTABILITY

Consider coupled oscillation of the proton beam and the electron 'beam' in the vertical direction. The displacements of a proton and electron from the central axis of the vacuum chamber are denoted, respectively, by y_p and y_e. Here, we assume both the proton and electron beams are coasting beams having the same transverse sizes and uniform distribution longitudinally and transversely. The coupled equations of motion are [11, 7, 4, 13]

$$\left(\frac{\partial}{\partial t} + \omega_0\frac{\partial}{\partial\theta}\right)^2 y_p + Q_\beta^2\omega_0^2 y_p = -Q_p^2\omega_0^2(y_p - \bar{y}_e) + Q_{ps}^2\omega_0^2(y_p - \bar{y}_p) , \quad (18.9)$$

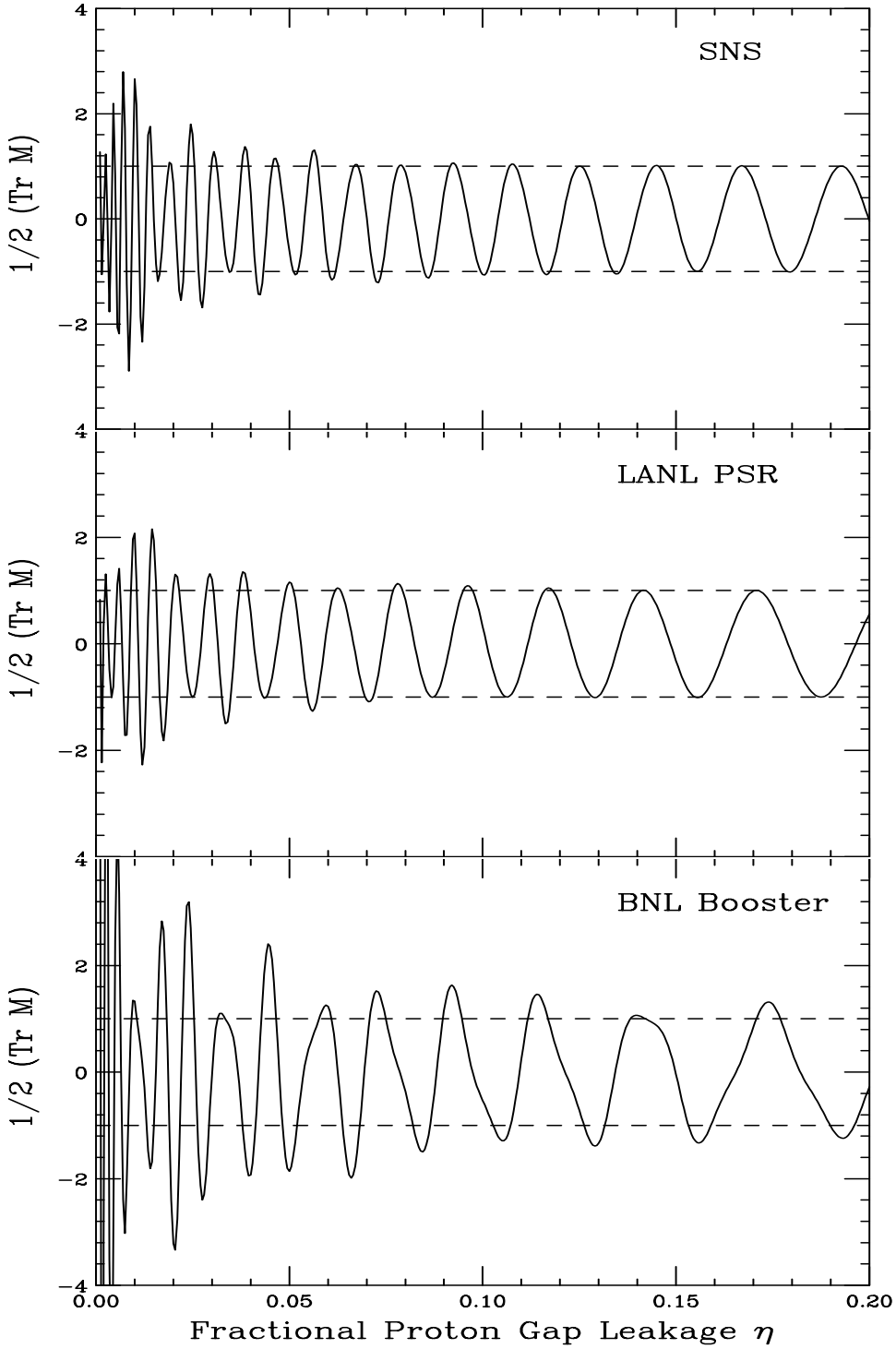

Figure 18.4: The ORNL SNS: Electrons will be trapped if $\frac{1}{2}\mathrm{Tr}M$ falls between the ± 1 dashed lines. The 3 plots are, from top down, for the ORNL SNS, LANL PSR, and BNL Booster.

$$\frac{d^2 y_e}{dt^2} = -Q_e^2 \omega_0^2 (y_e - \bar{y}_p) + Q_{es}^2 \omega_0^2 (y_e - \bar{y}_e) \ , \tag{18.10}$$

where $\bar{y}_p$ and $\bar{y}_e$ are the vertical displacements of the centroids of, respectively, the proton and electron beams from the axis of the vacuum chamber, ω_0 is the angular revolution frequency, θ is the azimuthal angle around the ring, Q_β is the betatron tune, and Q_p and Q_e are, respectively, the oscillation tune of the electrons inside the proton beam and the oscillation tune of the protons inside the electron beam. We have

$$\Omega_e^2 = (Q_e \omega_0)^2 = \frac{4 N_p r_e c^2}{a_{_V}(a_{_H} + a_{_V}) C} \ , \tag{18.11}$$

$$\Omega_p^2 = (Q_p \omega_0)^2 = \frac{4 N_p r_p c^2 \chi_e}{a_{_V}(a_{_H} + a_{_V}) \gamma C} \ , \tag{18.12}$$

where χ_e is the neutralization factor, or the ratio of the electron distribution to the proton distribution. In above, r_p is the classical proton radius, r_e the classical electron radius, and C the circumference of the accelerator ring. The negative signs on first terms on the right hand sides of Eqs. (18.9) and (18.10) indicate that the protons are focused by the electron beam and the electrons are focused by the proton beam. The factor γ in the denominator of Ω_p^2 comes about because the protons are circulating around the ring while the electrons do not. Notice that there are no magnetic force contributions. For Ω_e, the electron has no velocity although it sees a magnetic field from the proton beam. For Ω_p, the proton, although at a high velocity, does not see a magnetic field in the stationary electron beam. Again, we are considering uniformly and cylindrical-symmetrically distributed proton and electron beams of radius a; or $a_{_V}(a_{_H}+a_{_V}) \rightarrow 2a^2$. Image effects in the walls of the vacuum chamber as well as nonlinear focusing forces are neglected.

The last term in the proton equation denotes the oscillations of the proton under the self-field of the proton beam. Here,

$$(Q_{ps} \omega_0)^2 = \frac{4 N_p r_p c^2}{a_{_V}(a_{_H} + a_{_V}) \gamma^3 C} \tag{18.13}$$

is proportional to the linear space-charge tune shift of the proton beam. Similarly the last term in the electron equation, with

$$Q_{es}^2 = Q_e^2 \chi_e \tag{18.14}$$

denoting the space-charge tune shift of the electron beam, depicts the corresponding oscillations of the electron in the self-field of the electron beam.

Averaging over the proton displacements and electron displacements, we obtain the equations for the coupled motion of the proton-beam centroid $\bar{y}_p$ and the electron-beam centroid $\bar{y}_e$. Notice that the space-charge terms, Q_{ps}^2 and Q_{es}^2, drop out. If there is a coherent instability occurring at the angular frequency $\omega = Q\omega_0$, we can write

$$\bar{y}_p \sim e^{i(n\theta-\omega t)} \qquad \text{and} \qquad \bar{y}_e \sim e^{i(n\theta-\omega t)} \ , \tag{18.15}$$

where n is the longitudinal harmonic number. The coupled equations can be readily solved to give

$$(Q^2 - Q_e^2)[(n-Q)^2 - Q_\beta^2 - Q_p^2] - Q_e^2 Q_p^2 = 0 \ , \tag{18.16}$$

which is a quartic. For a solution when Q is near Q_e, we can expand Q around Q_e. When Q_p or the neutralization factor χ_e is large enough, the solution becomes complex and an instability occurs. The limiting Q_p for stability is given by

$$Q_p \lesssim \frac{|(n-Q_e)^2 - Q_\beta^2 - Q_p^2|}{2\sqrt{Q_e|n-Q_e|}} \ , \tag{18.17}$$

from which the limiting neutralization factor χ_e can be obtained. Once above threshold, the growth rate, given by

$$\frac{1}{\tau} = \frac{Q_p\omega_0}{2}\sqrt{\frac{Q_e}{|n-Q_e|}} \ , \tag{18.18}$$

is very fast. Notice that Q_p^2 on the right side of Eq. (18.17) in the numerator can be neglected because usually $Q_p^2 \ll Q_\beta^2$.

A proper employment of Eq. (18.17) is important, because it can give meaningless result. For example, in the situation:

$$[Q_e] = [Q_\beta] \qquad \text{or} \qquad [Q_e] + [Q_\beta] = 1 \ , \tag{18.19}$$

where $[Q_e]$ and $[Q_\beta]$ are, respectively, the residual betatron tune and the residual electron bounce tune, there will always exist a harmonic n which leads to instability for $Q_p \to 0$ or neutralization $\chi_e \to 0$. However, the growth rate will go to zero also. In reality, there is always a variation in the proton linear density or the electron bounce tune Q_e usually has a spread. Also the betatron tune can be suitably adjusted. For this reason, to estimate the threshold, we first compute Q_e from Eq. (18.11). Then the most offending harmonic n is determined as the integer closest to $Q_e + Q_\beta$. We next modify Q_e slightly so that

$$n - Q_e - Q_\beta = \frac{1}{2} \ . \tag{18.20}$$

Table 18.3: Coherent centroid-oscillation instability for proton-electron coasting beams.

	Oak Ridge SNS	Los Alamos PSR	Brookhaven Booster
Total number of protons N_p	2.10×10^{14}	4.2×10^{13}	4.42×10^{13}
Betatron tune Q_β	5.82	2.14	4.80
Proton beam radius a (m)	0.0380	0.0150	0.0150
$Q_p/\sqrt{\chi_e}$	1.2501	1.000	1.313
Most offending harmonic n	83	61	67
$Q_e = n - Q_\beta - \frac{1}{2}$	76.68	58.36	79.70
Limiting Q_p	0.1379	0.0963	0.1229
Limiting neutralization χ_e	0.0122	0.0093	0.0132
Growth rate in number of turns	0.663	0.703	0.668
Landau damping with $(\Delta Q_\beta - 2\Delta Q_{sc})/Q_\beta = 0.03$ and $\Delta Q_e/Q_e - \chi_e = 0.25$			
Limiting Q_p	0.5040	0.1853	0.4157
Limiting neutralization χ_e	0.1626	0.0343	0.151
Growth rate in number of turns	0.176	0.340	0.386

Notice that one can also determine n as the integer closest to $|Q_e - Q_\beta|$. However, the threshold neutralization will in general be higher than that obtained by the first method if a difference less than $\frac{1}{2}$ is used on the right side of Eq. (18.20).

With this consideration, the results are listed in Table 18.3. Here, the intensity of 4.42×10^{13} protons is used for the Brookhaven booster, where coasting beam experiments with possible e-p instabilities have been observed. We notice that the neutralization threshold is about 1.2% for the ORNL SNS, 0.9% for the LANL PSR, and 1.3% for the BNL booster. Once the thresholds are reached, the growth rates are very fast and the corresponding growth times are less than one turn for all the 4 machines.

There is another consideration of the stability of the two beam centroids, since the coherent oscillation can be stabilized by Landau damping. The equation of motion of the electron, Eq. (18.10), can be viewed as an undamped oscillator driven by $\bar{y}_p$, the centroid of the proton beam. Thus, spreads in the proton betatron tune Q_β and/or proton bounce tune Q_p alone will not be able to damp the electron oscillations. To damp the electron oscillation, there must be a spread in the electron bounce tune Q_e. The same applies to the equation of motion of the proton, Eq. (18.9), driven by the centroid of the electron

beam. Therefore, to provide Landau damping to the coupled-centroid oscillation, there must exist large enough spreads in both the betatron tune ΔQ_β and the electron bounce tune ΔQ_e.

First, we rewrite Eqs. (18.9) and (18.10) as

$$\left(\frac{\partial}{\partial t}+\omega_0\frac{\partial}{\partial\theta}\right)^2 y_p + Q_p'^2\omega_0^2 y_p = Q_p^2\omega_0^2\bar{y}_e - Q_{ps}^2\omega_0^2\bar{y}_p \ , \tag{18.21}$$

$$\frac{d^2 y_e}{dt^2} + Q_e'^2\omega_0^2 y_e = Q_e^2\omega_0^2\bar{y}_p - Q_{es}^2\omega_0^2\bar{y}_e \ , \tag{18.22}$$

where we have denoted

$$Q_p'^{\,2} = Q_\beta^2 + Q_p^2 + Q_{ps}^2 \qquad \text{and} \qquad Q_e'^{\,2} = Q_e^2 + Q_{es}^2 \ . \tag{18.23}$$

Second, with the ansatz in Eq. (18.15), the coupled differential equations becomes

$$y_p = \frac{-Q_p^2\bar{y}_e + Q_{ps}^2\bar{y}_p}{\left(Q-\dfrac{n\dot{\theta}}{\omega_0}\right)^2 - Q_p'^2} \ , \tag{18.24}$$

$$y_e = \frac{-Q_e^2\bar{y}_p + Q_{es}^2\bar{y}_e}{Q^2 - Q_e'^2} \ . \tag{18.25}$$

Third, we need to integrate both sides with the suitable distribution functions. In doing so, two approximations are to be made: (1) only the denominators of Eqs. (18.21) and (18.22) depend on the distributions which appear in differences of squares but not the numerator, and (2) only the *slow wave* will be included. It is then easy to obtain

$$\bar{y}_p = -\frac{Q_p^2}{2Q_p'\delta Q_p}\,\bar{y}_e + \frac{Q_{ps}^2}{2Q_p'\delta Q_p}\,\bar{y}_p \tag{18.26}$$

$$\bar{y}_e = +\frac{Q_e^2}{2Q_e'\delta Q_e}\,\bar{y}_p - \frac{Q_{es}^2}{2Q_e'\delta Q_e}\,\bar{y}_e \tag{18.27}$$

where

$$\delta Q_p'^{-1} = \int \frac{F_p(s)ds}{n - Q_p' - Q + \delta_p s} \tag{18.28}$$

$$\delta Q_e'^{-1} = \int \frac{F_e(s)ds}{Q_e' - Q + \delta_e s} \tag{18.29}$$

$$\delta_p = \frac{\partial}{\partial s}\left(Q'_p(s) - \frac{n\dot{\theta}(s)}{\omega_0}\right)_{s=0} \tag{18.30}$$

$$\delta_e = \left(\frac{\partial Q'_e(s)}{\partial s}\right)_{s=0} \tag{18.31}$$

and Q_p, Q'_p, Q_{ps}, Q_e, Q'_e, Q_{es} in Eqs. (18.26) to (18.29) are all evaluated at $s = 0$. Here, s being a generic variable, which can represent amplitude, momentum spread, etc, while $F_p(s)$ and $F_e(s)$ are distributions normalized to unity for the protons and electrons. From Eqs. (18.26) and (18.27), it is easy to get

$$\left(2\delta Q'_p + \frac{Q_{ps}^2}{2Q'_p}\right)\left(2\delta Q'_e + \frac{Q_{es}^2}{2Q'_e}\right) - \frac{Q_p^2 Q_e^2}{Q'_p Q'_e} = 0 \ . \tag{18.32}$$

Now following Laslett, *et al*, semi-circular distributions,

$$F_p(s) = \frac{2}{\pi s_{1/2p}^2}\sqrt{s_{1/2p}^2 - s^2} \qquad \text{and} \qquad F_e(s) = \frac{2}{\pi s_{1/2e}^2}\sqrt{s_{1/2e}^2 - s^2} \ , \tag{18.33}$$

are assumed for both the protons and electrons. One obtains

$$\begin{cases} 2\delta Q'_p = Q'_p - n + Q + i\bar{\Delta}_p \ , \\ 2\delta Q'_e = Q'_e + Q + i\bar{\Delta}_e \ , \end{cases} \tag{18.34}$$

where

$$\begin{cases} \bar{\Delta}_p = \sqrt{\Delta Q_p^2 - (Q - n + Q'_p)^2} \ , \\ \bar{\Delta}_e = \sqrt{\Delta Q_e^2 - (Q - Q'_e)^2} \ , \end{cases} \tag{18.35}$$

while ΔQ_p and ΔQ_e are the actual half spread of Q'_p and Q'_e in these distributions and are related to δ_p and δ_e in Eqs. (18.30) and (18.31) by

$$\Delta Q_p = s_{1/2p}\delta_p = s_{/2p}\frac{\partial}{\partial s}\left(\frac{Q'_p(s) - n\dot{\theta}(s)}{\omega_0}\right)_{s=0} \tag{18.36}$$

$$\Delta Q_e = s_{1/2e}\delta_e = s_{1/2e}\left(\frac{\partial Q'_e}{\partial s}\right)_{s=0} \tag{18.37}$$

Substitution into Eq. (18.32) leads to a quadratic equation in the coherent coupled-oscillation tune Q, the solution of which is

$$Q = Q'_e + \frac{Q_{es}^2}{Q'_e} + d_1 - \frac{i}{2}(\bar{\Delta}_e + \bar{\Delta}_p) \pm i\left\{\frac{Q_p^2 Q_e^2}{Q'_p Q'_e} - \left[d_1 - \frac{i}{2}(\bar{\Delta}_e - \bar{\Delta}_p)\right]^2\right\}^{1/2} \ , \tag{18.38}$$

where

$$d_1 = \frac{1}{2}\left[\left(n - Q'_p - \frac{Q_{ps}^2}{Q'_p}\right) - \left(Q'_e + \frac{Q_{es}^2}{Q'_e}\right)\right] \ . \tag{18.39}$$

It is clear that stability requires in Eq. (18.38)

$$\mathcal{R}e\left\{ \quad \right\} \geq \frac{1}{2}\left(\bar{\Delta}_e + \bar{\Delta}_p\right) \ . \tag{18.40}$$

This criterion is equivalent to, after considerable amount of algebra,

$$\bar{\Delta}_p\bar{\Delta}_e \geq \frac{Q_p^2 Q_e^2}{Q'_p Q'_e}\left[1 + \left(\frac{2d_1}{\bar{\Delta}_p + \bar{\Delta}_e}\right)^2\right]^{-1} \ . \tag{18.41}$$

Within a narrow band of instability, associated with the resonance $d_1 \approx 0$, or $n - Q'_p - Q \approx Q_{ps}^2/Q'_p$ and $|Q'_e - Q| \approx Q_{es}^2/Q'_e$, the stability limit can be simplified. With the substitution of Eq. (18.35), we finally arrive at

$$\left[\Delta Q_p^2 - \left(\frac{Q_{ps}^2}{Q'_p}\right)^2\right]^{1/2}\left[\Delta Q_e^2 - \left(\frac{Q_{es}^2}{Q'_e}\right)^2\right]^{1/2} \geq \frac{Q_p^2 Q_e^2}{Q'_p Q'_e} \ . \tag{18.42}$$

Because square roots are involved, we also require

$$\Delta Q_p > \left|\frac{Q_{ps}^2}{Q'_p}\right| \qquad \text{and} \qquad \Delta Q_e > \left|\frac{Q_{es}^2}{Q'_e}\right| \ . \tag{18.43}$$

It is important to point out that the space-charge self-force terms of Eqs. (18.9) and (18.10) do not drop out when averaged over the distributions. As an approximation, $Q'_p \sim Q_\beta$ implying that $Q_{ps}^2/Q'_p \sim 2\Delta Q_{sc}$, where ΔQ_{sc} is the linear space-charge tune shift of the proton beam. Similarly, we can write $Q_{es}^2/Q'_e \sim Q_e\chi_e$, which is twice the linear space-charge tune shift of the electron beam. The stability condition then simplifies to

$$\left[\Delta Q_\beta^2 - 4\Delta Q_{sc}^2\right]^{1/2}\left[\Delta Q_e^2 - \chi_e^2 Q_e^2\right]^{1/2} \gtrsim \frac{Q_p^2 Q_e}{Q_\beta} \ . \tag{18.44}$$

Because of the square roots on the left side of Eq. (18.44), we also require for stability,

$$\Delta Q_\beta \geq 2Q_{sc} \qquad \text{and} \qquad \frac{\Delta Q_e}{Q_e} \geq \chi_e \ . \tag{18.45}$$

The spread in the electron bounce frequency is difficult to measure. However, when instability occurs, the electron bounce frequency is very close to the coherent instability

frequency, which is the same for the proton beam and the electron. Thus measuring the coherent transverse oscillation frequency of the proton beam, we can infer the electron bounce frequency. According to the measurement at PSR, $\Delta Q_e/Q_e \sim 0.25$. Assuming that the neutralization factor is small, we may set the half maximum fractional spread of the electron bounce tune to be $\Delta Q_e/Q_e - \chi_e \sim 0.1$, and the half maximum fractional spread of the betatron tune in excess of twice the space-charge tune shift is $(\Delta Q_\beta - 2\Delta Q_{sc})/Q_\beta \sim 0.03$. The limiting Q_p and neutralization factor χ_e can now be computed and are also listed in Table 18.3. For the ORNL SNS and the Brookhaven booster, the threshold neutralization factors have been increased to 16.3% and 15.1%, respectively, which are more than 10 times. For the LANL PSR, however, the neutralization threshold χ_e becomes $\sim 3.4\%$, an increase of less than 4 times. Further increase in threshold requires larger spreads in Q_e and Q_β. In fact, it has been demonstrated that anti-damping can even happen unless there is a large enough overlap between ΔQ_β and ΔQ_e [11]. Notice that these stability limits of the neutralization factor can be sensitive to the distributions of the betatron tune and the electron bounce tune.

A stability condition has also been derived by Schnell and Zotter [11] assuming parabolic distributions for the betatron tune and the electron bounce tune, but without consideration of the space-charge self-forces. They obtain

$$\frac{\Delta Q_\beta}{Q_\beta}\frac{\Delta Q_e}{Q_e} \gtrsim \frac{9\pi^2}{64}\frac{Q_p^2}{Q_\beta^2} \,. \tag{18.46}$$

Notice that the Schnell-Zotter criterion is essentially the same as the Laslett-Sessler-Möhl criterion, if we interpret ΔQ_β of the former as the half tune spread of the betatron tune *in excess* of twice the space-charge tune spread of the proton beam, and ΔQ_e as the half tune spread of the electron bounce tune *in excess* of twice the space-charge tune spread of the electron beam. The factor $9\pi^2/64$ in Eq. (18.46) is probably a form factor of the parabolic distributions. Our discussion can be generalized when we notice that both Q_{ps}^2/Q_p' and Q_{es}^2/Q_e' in Eq. (18.42) come from, respectively, the $\bar{y}_e$ term in Eq. (18.9) and the $\bar{y}_p$ term in Eq. (18.10). Thus, Q_{ps}^2 and Q_{es}^2 can be extended to include the perturbations of oscillations coming from all types of impedances of the accelerator ring. In that case, the Schnell-Zotter stability criterion should be valid if we interpret ΔQ_β as the half tune spread of the betatron tune in excess of what is necessary to cope with the instabilities of the single proton beam, and ΔQ_e as the half tune spread of the electron bounce tune in excess of what is necessary to cope with the instabilities of the single electron beam.

18.4 PRODUCTION OF ELECTRONS

As seen in the previous section, the e-p coherent centroid-oscillation instability depends strongly on the neutralization factor, or the amount of electrons trapped inside the proton bunch.

One source of electron production is through collision of the protons with the residual gas in the vacuum chamber. At a vacuum pressure of 1×10^{-7} Torr, there is a residual gas density of $n_{\rm res} = 3.2 \times 10^9$ molecules/cm^3. The expected average ionization cross section is $\sigma_i = 1.2 \times 10^{-18}$ cm^2. If the residual gas is mostly bi-atomic molecules, each contributing two electrons, the rate of electron production is [9]

$$\frac{dN_e}{dt} = 2\beta c n_{\rm res} \sigma_i N(t) \ , \tag{18.47}$$

where $N(t)$ is the number of protons accumulated from injection at time t. If $t_{\rm inj}$ is the total injection time, $N(t) = N_p t/t_{\rm inj}$, where N_p is the total number of protons at the end of the injection. The neutralization due to ionization collision at the end of injection is therefore

$$\chi_e = \frac{N_e}{N_p} = \beta c n_{\rm res} \sigma_i t_{\rm inj} \ . \tag{18.48}$$

The vacuum pressure for the ORNL SNS is designed to be 1×10^{-9} Torr and that for the LANL PSR is 2×10^{-8} Torr, while the other ring is with vacuum pressure 1×10^{-7} Torr. The neutralization due to ionization collision turns out to be 0.104%, 1.39%, and 2.33%, respectively, for the ORNL SNS, LANL PSR, and BNL booster. The neutralization factors are large for PSR and the BNL booster because of their relatively low vacuum and long injection times of, respectively, ~ 2000 and 300 turns. The maximum neutralization of the ORNL SNS is small because of the very high vacuum.

Another source of electron production is through the multi-traversing of the stripping foil by the proton beam. For example, a proton in the LANL PSR can generate on the average two electrons because of the presence of the stripping foil.

A more important source of electron production is when an electron hitting the walls of the beam pipe releases secondary electrons. These secondary electrons can cause multipactoring and generate a large amount of electrons. Here, we would like to compute the energy of an electron hitting the beam pipe and estimate the efficiency of secondary emission [10].

An electron is oscillating with bounce frequency $\Omega_e/(2\pi)$ with amplitude increasing

exponentially with an e-folding growth rate ω_I. Assume that the electron just grazes the wall of the beam pipe at time $t = 0$. Its amplitude is given by

$$y = be^{\omega_I t} \cos \Omega_e t \ , \tag{18.49}$$

where b is the beam pipe radius. It will hit the other side of the wall at time $t_1 = (\pi - \Delta)/\Omega_e$, where

$$-b = be^{\omega_I t_1} \cos \Omega_e t_1 = be^{(\pi-\Delta)\omega_I/\Omega_e} \cos(\pi - \Delta) \ , \tag{18.50}$$

which leads to

$$\Delta = \sqrt{\frac{2\pi\omega_I}{\Omega_e}} \left[1 + \mathcal{O}\left(\sqrt{\frac{\omega_I}{\Omega_e}}\right)\right] \ . \tag{18.51}$$

The velocity of the electron hitting the other side of the wall can be obtained by differentiating Eq. (18.49) and is given by

$$\dot{y} = b\sqrt{2\pi\omega_I\Omega_e} \left[1 + \mathcal{O}\left(\sqrt{\frac{\omega_I}{\Omega_e}}\right)\right] \ . \tag{18.52}$$

The kinetic energy is therefore

$$E_{\rm kin} = \pi m_e \omega_I \Omega_e b^2 \ , \tag{18.53}$$

where m_e is the electron mass.

For single-electron motion, we can identify the growth rate $\omega_I = \mu\beta c/\lambda_{\rm rf}$, where μ is given by Eq. (18.4). The velocities and kinetic energies of the electrons hitting the wall on the other side of the beam pipe are listed in Table 18.4. We see that when hitting the beam pipe wall, the electrons possess kinetic energies of 198.6, 775.4, and 139.5 eV, respectively, for the 3 rings. For the BNL booster, the bunched mode intensity has been used. It is a known fact that an electron in excess of 100 eV hitting a metallic wall will result in a secondary emission coefficient greater than unity. This implies that multipactoring will occur in these rings. This consideration is for the motion of a single electron and is independent of the amount of electrons present in the ring. In the design of the ORNL SNS, the beam pipe will be made of stainless steel with a titanium coating, which will reduce the secondary emission efficiency and thus prevent multipactoring to occur. An experiment was performed at the LANL PSR by coating part of the walls of the vacuum chamber with TiN. The electron flux was found to have been suppressed about 1000 times [14].

We can also identify ω_I with the growth rate τ^{-1} of the coherent centroid oscillation in Eq. (18.18). The kinetic energy for an electron hitting the other side of the beam pipe

Table 18.4: Kinetic energy of electron hitting the wall of the beam pipe.

	Oak Ridge SNS	Los Alamos PSR	Brookhaven Booster
Total number of protons N_p	2.1×10^{14}	4.2×10^{13}	2.4×10^{13}
Beam pipe radius b (m)	0.0500	0.0500	0.0600
Single-electron consideration			
Electron escaping rate ω_I (MHz)	6.24	13.9	4.69
Ω_e (MHz)	713.3	1253.9	462.6
Velocity hitting wall $\dot{y}/c$	0.0279	0.0551	0.0234
Kinetic energy hitting wall (eV)	198.6	775.4	139.5
Coherent-centroid-oscillation consideration			
Threshold neutralization χ_e	0.0122	0.0093	0.0066
Growth rate ω_I (MHz)	1.793	3.976	0.644
Ω_e (MHz)	572.7	1025.2	554.6
Velocity hitting wall $\dot{y}/c$	0.0134	0.0267	0.0095
Kinetic energy hitting wall (eV)	4.62	182.9	23.0

wall becomes

$$E_{\rm kin} = \frac{\pi m_e Q_p Q_e^{3/2} \omega_0^2 b^2}{2\sqrt{|n - Q_e|}} \ . \tag{18.54}$$

Notice that the kinetic energy of the electron hitting the pipe wall is now proportional to Q_p and therefore $\sqrt{\chi_e}$. These are listed in Table 18.4 at the threshold neutralization. Notice that the kinetic energies of the electrons hitting the beam pipe walls at the onset of coupled-centroid instability are less than 100 eV for the ORNL SNS and the BNL booster in the bunched mode. Thus multipactoring will occur only if the neutralization factor is much larger than $\sim 1\%$. On the other hand, the electron kinetic energy is 182 eV for the PSR. Thus multipactoring will occur before the onset of coherent centroid instability.

18.5 BOUNCE FREQUENCY

E-p instability is different from other transverse instability in that the bounce frequency of the electrons inside the proton bunch is very broad. Recall that the angular

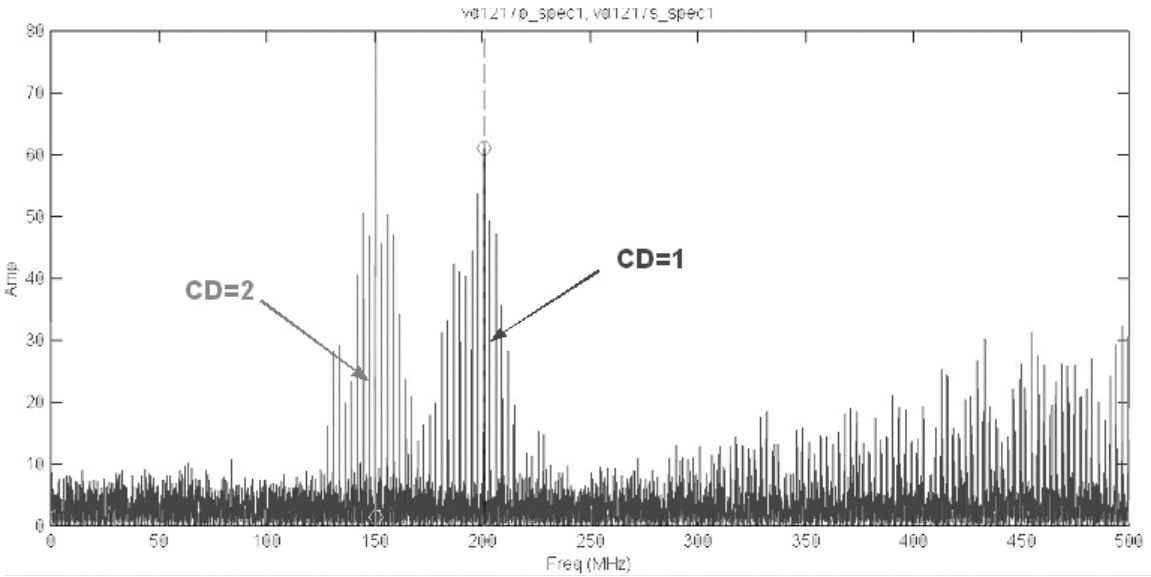

Figure 18.5: The PSR is run at CD 1 with 6.1 μC. The electron bounce frequency is measured to be centered at $\sim$ 200 MHz, close to the theoretical prediction. The total spread of the bounce frequency is roughly 100 MHz, the same order of magnitude as its center value. Operated at CD 2 with 3.0 μC, the bounce frequency reduces to $\sim$ 140 MHz, roughly by $\sqrt{2}$ times as expected.

bounce frequency is defined as

$$\Omega_e = \sqrt{\frac{4\lambda r_e c^2}{a_V(a_V + a_H)}} \; . \tag{18.55}$$

where λ is the linear particle density of the proton bunch. Thus, the bounce frequency of the electrons depends on where they are inside the proton bunch. For example, if the electrons are trapped within the proton FWHM bunch profile, the spread of the bounce frequency will be $1/\sqrt{2}$ its mean value, which is certainly a wide spread. Another test of the e-p bounce oscillation is to measure the dependency of the bounce frequency on the proton beam intensity. As is given by Eq. (18.55), the bounce frequency should be proportional to the square root of the proton intensity. Such a measurement has been performed at the Los Alamos PSR and is shown in Fig. 18.5. At countdown 1 (CD 1), the longest chopped proton beam is injected from the linac. At 6.1 μC or 3.81×10^{13} proton injected, the electron bounce frequency observed is $\sim$ 200 MHz, very close to the prediction of Eq. (18.55). Next the injection is at countdown 2 (CD 2), where the chopped beam from the linac is injected into the PSR on alternate turns, thus reducing the total

injection intensity by half to 3.0μC. The bounce frequency is found to peak at $\sim$ 140 MHz, very close to a reduction of $\sqrt{2}$ as predicted. The total spread of the bounce frequency at CD 1 is about 100 MHz, which is also the same order of magnitude as predicted above.

18.6 DISCUSSIONS AND CONCLUSION

(1) In the above single-electron analysis, it appears that electrons will be cleared in the bunch gap within one rf wavelength for all the 3 proton rings under consideration. However, if more than $\eta \sim 4\%$ of the protons are spilled into the bunch gap, electrons will be trapped inside the proton beam in the ORNL SNS and LANL PSR. For the BNL booster, on the other hand, electrons are relatively more difficult to be trapped when there are spilled protons in the bunch gaps even if $\eta > 20\%$. This is probably due to its much larger gap-to-bunch-length ratio.

(2) For coherent centroid oscillation to become unstable, neutralization factors of $\chi_e \sim 1.2\%$, 0.9%, and 1.1% are required, respectively, for the three machines. However, spreads in the betatron frequencies and the electron bounce frequencies can provide Landau damping.

(3) The LANL PSR may accumulate protons through an injection in $\sim$ 2000 turns and the BNL Booster in 300 turns. The vacuum pressures of both rings are relatively high, $\sim 1 \times 10^{-8}$ Torr for the former and $\sim 1 \times 10^{-7}$ Torr for the latter. As a result, the amount of electrons per proton produced by collision with residual gases can be as high as 1.39 and 2.33%, respectively, for the two rings. However, the electron production for the ORNL SNS via proton-ion collision is less than 1%, which is the result of a high vacuum of 1×10^{-9} Torr in the vacuum chamber.

(4) Multipactoring as a result of secondary emission will be possible for all the three rings when single electron escapes from the trapping proton beam and hits the metallic beam pipe. For the LANL PSR, multipactoring will occur before the onset of coherent centroid instability. However, for the other two rings, multipactoring will not occur as soon as centroid oscillations become unstable.

(5) There is a similar proton ring called ISIS at the Rutherford Appleton Laboratory. At the injection energy of 70.4 MeV, about 2.5×10^{13} protons are stored as a continuous coasting beam, which is then captured adiabatically into 2 rf buckets. The protons are

ramped to 0.8 GeV when they are extracted. No e-p instabilities have ever been observed at ISIS either running in the bunched mode or the coasting-beam mode. This has always been a puzzle. However, when we compare ISIS with the LANL PSR, we do find some important differences. First, ISIS has a repetition rate of 50 Hz. The injection is fast, about 200 turns. On the other hand, it usually takes about 200 turns for the e-p instability of the PSR to develop to a point when it can be monitored. Second, ISIS has a much larger vacuum chamber, 7 cm in radius. Also the ISIS vacuum chamber is made of ceramic to limit eddy current because of the high repetition rate of 50 Hz. However, a wire cage is installed inside the ceramic beam pipe to carry the longitudinal return current. The wire cage does not allow transverse image current to flow, thus alleviating in some way the transverse instability. Also the cage wires have much less surface area than the walls of an ordinary metallic beam pipe. As a result, secondary emission will be reduced. The secondary emitted electrons will come out in all directions from the cage wires. The probability for them to hit another cage wire will be small, thus preventing multipactoring to occur. These may be the reasons why e-p instabilities have never been observed at ISIS.

18.7 EXERCISES

18.1. Modify the coupled proton and electron equations of motion [Eqs. (18.9) and (18.10)] by including the influence of an infinitely conducting cylindrical beam pipe of radius b. Without taking into account the distributions of the various tunes, solve the equations for the threshold of coupled-centroid instability [similar to Eq. (18.17)] and the initial growth rate [similar to Eqs. (18.17) and (18.18)].

18.2. Derive in detail Eq. (18.54) for the kinetic energy of an electron hitting the wall of the beam pipe after it grazes the opposite wall.

18.3. In the experiment for measuring coupled-centroid instability at the Los Alamos PSR, the bunch occupies 2/3 of the circumference of the storage ring. The coherent frequency which is close to the electron bounce frequency at CD 1 or 6.1 μC is shown in Fig. 18.5. Other information of the PSR are listed in Table 18.1.
(1) Assuming a parabolic linear distribution of the proton bunch, and the maximum coherent or bounce frequency of 240 MHz, estimate the transverse size of the proton beam.
(2) From the peak value of the bounce frequency, estimate the location along the proton beam where the electron density is at a maximum.

18.4. Fermilab is proposing a new high intensity booster having circumference 711.304 m with rf harmonic 4. Protons are injected at the kinetic energy of 400 MeV to an intensity of 8.6×10^{12} per bunch. At the end of injection, each proton bunch has a uniform linear density but is occupying 2/3 of the rf bucket. The transverse cross section of the beam is circular with a radius of 2.35 cm.
(1) Assuming the bunch gap is totally clean, show that electrons will not be trapped inside the proton beam.
(2) If a fraction η of protons is spilled into the bunch gaps, compute the minimum η that will lead to electron trapping.

18.5. Starting from the equations of coupled transverse motion, Eqs (18.9) and (18.10), assuming circular distributions for the protons and electrons, derive the Laslett-Sessler-Möhl stability criterion, Eq. (18.42).

Bibliography

[1] H. Grunder, G. Lambertson, Proc. VIII Int. Conf. on High Energy Accel., p.308 (1971).

[2] H.G. Herewards, CERN Report CERN-71-15, (1971).

[3] R. Macek, *Overview of New Developments on the PSR Instability*, Proceedings of 8th Advanced Beam Dynamics Mini-Workshop on Two-Stream Instabilities in Particle Accelerators and Storage Rings, Santa Fe, Feb. 16-18, 2000, web site: http://www.aps.anl.gov/conferences/icfa/proceedings.html.

[4] M. Blaskiewicz, *The Fast Loss Electron Proton Instability*, Proceedings of the Workshop on Instabilities of High Intensity Hadron Beams in Rings, ed. T. Roser and S.Y. Zhang, Upton, N.Y., 1999, p. 321; *Estimating Electron Proton Instability Thresholds*, Proceedings of 8th Advanced Beam Dynamics Mini-Workshop on Two-Stream Instabilities in Particle Accelerators and Storage Rings, Santa Fe, Feb. 16-18, 2000, web site: http://www.aps.anl.gov/conferences/icfa/proceedings.html.

[5] J. Rosenzweig and P. Zhou, *Coherent Beam-ion Instabilities in the Fermilab Antiproton Accumulator*, *Ion Trapping in the Tevatron with Separated Orbits*, *Ion Clearing Using Cyclotron Shaking*, Proceedings of Fermilab III Instabilities Workshop, Fermilab, Batavia, Ed. S. Peggs and M. Harvey, June 25-29, 1990, p. 9, 26, and 39.

[6] K. Harkay, *Electron Cloud Effects at APS*, Proceedings of 8th Advanced Beam Dynamics Mini-Workshop on Two-Stream Instabilities in Particle Accelerators and Storage Rings, Santa Fe, Feb. 16-18, 2000, web site: http://www.aps.anl.gov/conferences/icfa/proceedings.html.

[7] D. Neuffer, E. Colton, D. Fitzgerald, T. Hardek, R. Hutson, R. Macek, M. Plum, H. Thiessen, and T.-S.Wang, Nucl. Instr. Meth. **A321**, 1 (1992).

[8] In the reference below, aluminum pipe with titanium coating is mentioned: http://www.ornl.gov/∼nsns/CDRDocuments/CDRSections/CDRSections.html. In the more recent design, however, stainless steel beam pipe with TiN coating is used.

[9] A. Ruggiero and M. Blaskiewicz, *e-p Instabilities in the NSNS Accumulator Ring*, Proceedings of the 1999 Particle Accelerator Conference, New York, 1999, p.1581.

[10] M. Blaskiewicz, *Instabilities in the SNS*, Proceedings of the 1999 Particle Accelerator Conference, New York, 1999, p.1611.

[11] W. Schnell and B. Zotter, CERN Report ISR-GS-RF/76-26 (1976).

[12] L.J. Laslett, A.M. Sessler and D. Möhl, Nucl. Inst. Meth. **121** 517 (1974).

[13] Tai-Sen F. Wang, *A Theoretical Study of Electron-Proton Instability I and II*, LANL Report PSR-96-004 and PSR-96-004 (1996).

[14] R. Macek, talk given at the 8th Advanced Beam Dynamics Mini-Workshop on Two-Stream Instabilities in Particle Accelerators and Storage Rings, Santa Fe, New Mexico, February 16-18, 2000